

Transformer-based model for monocular visual odometry: a video understanding approach

André O. França^{a,*}, Marcos R. O. A. Maximo^a

^a*Autonomous Computational Systems Lab, Aeronautics Institute of Technology, Praça Marechal Eduardo Gomes, 50, São José dos Campos, 12228-900, Brazil*

Abstract

Estimating the camera pose given images of a single camera is a traditional task in mobile robots and autonomous vehicles. This problem is called monocular visual odometry and it often relies on geometric approaches that require engineering effort for a specific scenario. Deep learning methods have shown to be generalizable after proper training and a considerable amount of available data. Transformer-based architectures have dominated the state-of-the-art in natural language processing and computer vision tasks, such as image and video understanding. In this work, we deal with the monocular visual odometry as a video understanding task to estimate the 6-DoF camera's pose. We contribute by presenting the TSformer-VO model based on spatio-temporal self-attention mechanisms to extract features from clips and estimate the motions in an end-to-end manner. Our approach achieved competitive state-of-the-art performance compared with geometry-based and deep learning-based methods on the KITTI visual odometry dataset, outperforming the DeepVO implementation highly accepted in the visual odometry community.

Keywords: monocular visual odometry, deep learning, video understanding

1. Introduction

Determining the location of a robot in an environment is a classical task in mobile robots and autonomous vehicles applications [1]. Visual odometry (VO) consists of estimating the camera's pose and motion given a sequence of frames, i.e. using visual sensors. In the monocular case, the system has a single camera to capture the images. Consequently, there is a lack of depth information when the three-dimensional (3D) objects are projected into a two-dimensional (2D) space. Among the approaches to address the monocular VO, there are traditional geometry-based methods [2, 3], deep learning-based methods that use end-to-end architectures [4, 5], and hybrid methods with deep learning in certain modules of the geometry-based methods [6, 7, 8].

Although traditional methods are robust and well-developed, they must be fine-tuned properly to achieve high performance, i.e. there is a requirement for an engineering effort for each specific application [4]. Fur-

thermore, monocular VO systems suffer from scale ambiguity due to the lack of depth. The scale drift caused by the accumulation of scale errors during the motion estimation over time can be reduced via additional sensors or some supplementary information [1]. On the opposing side, end-to-end approaches can estimate the 6 degrees of freedom (DoF) poses directly from a sequence of RGB images, that is, it does not need engineering effort to project the modules in the traditional VO pipeline [4]. However, its performance is strongly dependent on a large and diverse training data to make the model robust and reliable, which is typical of deep learning approaches.

In recent years, the Transformer architecture [9], which is a deep learning method based on attention mechanisms, has been the basis of the state-of-the-art architectures in natural language processing (NLP) tasks, outperforming models based on recurrent neural networks (RNN) with long short-term memory cells (LSTM). After the success of transformer-based architectures such as BERT [10] and GPT [11], researchers started to apply the Transformer network to vision problems, reaching state-of-the-art performance on several image recognition benchmarks with the vision Transformer (ViT) model [12]. Furthermore, transformer-

*Corresponding author:

Email addresses: andre.francani@ga.ita.br (André O. França), mmaximo@ita.br (Marcos R. O. A. Maximo)

based architectures also achieved state-of-the-art results on video understanding tasks [13, 14].

In this article, we propose an end-to-end architecture based on Transformer. We treat the visual odometry as a video understanding problem, where the 6-DoF camera’s poses are estimated directly from a sequence of raw images. This approach is promising once visual odometry depends on spatio-temporal features, and transformer-based models have shown outstanding results on NLP tasks. We choose the TimeSformer [14] model for this work since it achieved state-of-the-art results in video action recognition tasks compared to previous works based on convolutional neural networks (CNN). In contrast to the original work, our idea is to use an MSE loss to perform a regression instead of classification, together with a proper post-processing step to recover the pose estimation from overlapped-windowed data. We conducted experiments on the model hyperparameters and showed that our approach achieved competitive results on the KITTI odometry benchmark. The main contributions of this work are summarized as follows:

- We present a video understanding perspective for monocular visual odometry tasks.
- We propose the TSformer-VO: an end-to-end architecture based on the TimeSformer model that estimates the 6-DoF camera’s pose.
- We show that our approach achieves competitive results on the KITTI odometry benchmark compared to previous works, outperforming a state-of-the-art method based on deep learning.
- The source code as well as the pre-trained models are available at <https://github.com/aofrancani/TSformer-VO>.

The remaining of this paper is organized as follows. Section 2 presents related works in monocular visual odometry, showing methods based on geometry and deep learning, as well as presenting the video understanding task. Section 3 introduces the proposed method and all required pre-processing and post-processing steps to estimate the 6-DoF camera’s poses. Section 4 defines the experimental setups of our experiments, presenting the results and their discussions. Finally, Section 5 establishes the overall conclusions of our work.

2. Related work

In this Section, we introduce the monocular visual odometry methods based on geometry and deep learn-

ing, as well as the state-of-the-art methods for the video understanding problem.

2.1. Monocular visual odometry

Monocular visual odometry estimates incrementally the motion of an agent using a sequence of frames captured from a single camera attached to this agent [1]. The motion can be estimated from geometry constraints, or estimated from a deep learning approach without engineering modeling of the scenario.

2.1.1. Geometry-based methods

In general, geometry-based algorithms follow the pipeline depicted in Fig. 1. Firstly, features or keypoints are detected in a frame, usually edges and corners. These features are matched and tracked to the subsequent frame using a similarity measurement. With the matched keypoints in successive frames, the essential matrix can be estimated using epipolar constraints. Then, the rotation matrix and translation vector are obtained by decomposing the essential matrix. Finally, the camera poses can be refined through an offline local optimization, such as bundle adjustment [1].

LIBVISO2 [15] is a known implementation of the traditional pipeline for the monocular and stereo cases. The monocular system uses an 8-point algorithm to estimate the essential matrix, and it assumes that the camera has a fixed height over the ground for estimating the scale. Another traditional state-of-the-art algorithm based on features and geometry is ORB-SLAM [16]. It uses ORB keypoints and a mapping system that enables it to recognize places and compute local and global optimization.

2.1.2. Deep learning methods

End-to-end deep learning-based methods estimate the 6-DoF of a camera pose given a sequence of images. It has neither the feature detection and matching steps nor the geometry constraints. The main idea is to extract features from images like a common computer vision task, and use them for regression to estimate the camera pose.

DeepVO [4] is a state-of-the-art end-to-end architecture that extracts features from an image pair (consecutive frames) using a CNN with pre-trained FlowNet weights [17], followed by an RNN with LSTM cells to handle the temporal information of the estimated poses. DeepVO achieved competitive results compared to geometry-based methods without the need for parameter tuning of traditional VO systems. A similar model called UnDeepVO [5] uses an unsupervised learning



Figure 1: Traditional pipeline for visual odometry.

technique to estimate the depth of the frames and use it to recover the scale. The depth and scale are obtained by stereo images during training, however, only monocular images are used during the test, making the system monocular.

2.2. Video understanding

Video understanding comprehends the recognition and localization of actions or events in videos. A typical task is called action recognition, which consists of assigning a single action to a clip. It is also possible to detect more than one action in videos, by classifying the actions in bounding boxes, similar to object detection problems.

SlowFast networks [18] are high-performance networks for video understanding tasks. It has a fast path that captures motion with high temporal resolution (input with a high frame rate), and a slow path that captures spatial features at a low frame rate. This family of networks might be cumbersome in terms of inference cost, measured by the number of multiply-add operations (FLOPs). This motivated the X3D architectures [19] that explore the expansion of a 2D image model along time, space, depth, and width axes. The X3D models achieved competitive performance compared with SlowFast architectures while requiring fewer FLOPs, i.e. being lighter in terms of the number of parameters.

Following the success of the Transformer architecture over convolutional networks in vision tasks, researchers explored the Transformer to extract spatio-temporal features in video understanding tasks. The TimeSformer [14] model extracts spatio-temporal features using the Transformer architecture over space and time, achieving state-of-the-art results on action recognition benchmarks. It is an extension of the ViT applied to the space-time volume, where the video is converted into a sequence of patches embedded through a linear map with added positional information. Different designs of the self-attention blocks in TimeSformer were investigated: space attention, joint space-time attention,

divided space-time attention, sparse local global attention, and axial attention. A competitive architecture is the ViViT [20] that explored different ways of extracting spatio-temporal features similar to TimeSformer.

In our work, we explore the divided space-time attention to estimate the 6-DoF pose in monocular visual odometry tasks, since this architecture is designed for computational efficiency while keeping the performance compared to other architectures. To the best of our knowledge, our work is the first to use a Transformer-based architecture in an end-to-end manner with a video understanding model to deal with the monocular visual odometry task.

3. Proposed method

This section introduces the proposed method, the pre-processing, and the post-processing step of our methodology. The architecture extracts spatio-temporal features with a self-attention mechanism to estimate the 6-DoF camera’s pose. As pre-processing, the ground truth absolute coordinates are converted to relative between time steps. Besides, the ground truth rotation matrix is represented as Euler angles. The post-processing involves reversing the transformations done in the pre-processing step, as well as adjusting the estimated motions that occur repeatedly due to the overlapped input clips.

3.1. TSformer-VO

The TSformer-VO model is based on the TimeSformer architecture for action recognition [14]. We applied a regression loss to estimate the 6-DoF pose of the input clip and explored the divided space-time self-attention blocks in our context. Fig. 2 illustrates schematically the steps employed in this architecture.

The input clip $\mathbf{X} \in \mathbb{R}^{N_f \times C \times H \times W}$ consists of N_f frames of size $C \times H \times W$ in the channel first setup. Each clip is decomposed into N patches of size $P \times P$, giving $N = HW/P^2$ non-overlapping patches. In sequence, each patch is flattened into a vector $\mathbf{x}_{(s,t)} \in \mathbb{R}^{CP^2}$, where

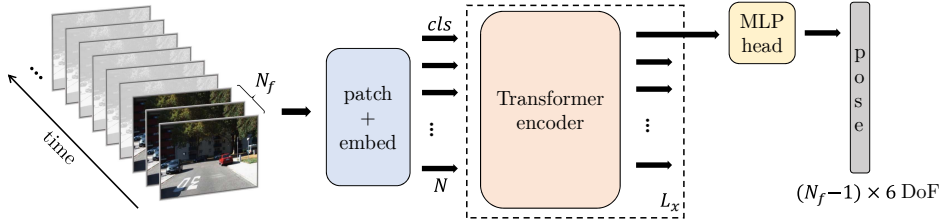


Figure 2: TSformer-VO pipeline. The input clips with N_f frames are processed into N patches. Each patch is embedded into tokens and is sent to the sequence of Transformer blocks. A special vector called class token (cls) gathers the information from all patches and passes through the final MLP head, outputting the 6-DoF for the $N_f - 1$ estimated poses.

s denotes the spatial locations, and t denotes the index over the frames in the clip. Each patch vector is embedded into tokens by a linear learnable map, equivalent to a 2D convolution. The output of this projection is the input token of the Transformer encoder. Those steps of decomposing into patches and embedding into tokens are traditional procedures introduced in [12].

Furthermore, we added the learnable positional embedding to each input token, and we follow the BERT Transformer [10] by adding a special learnable vector as the very first input token, known as class token. Although the name classification token is used, in our context we are not dealing with a classification problem, like in image classification and action recognition tasks. However, the idea of keeping this special parameter is to gather the information from all patches, avoiding the bias of choosing the output of a specific patch to pass through the multilayer perceptron (MLP) head.

Therefore, the final 1D input tokens are denoted as $\mathbf{z}_{(s,t)}^l \in \mathbb{R}^{E_d}$, where E_d is the embedding dimension of the flattened patch $\mathbf{x}_{(s,t)}$ at encoding block l . The final model has L_x encoder blocks stacked on top of each other.

There are mainly two different self-attention architectures to extract spatio-temporal features defined in [14]: “joint space-time” and “divided space-time”. In “joint space-time” self-attention, all spatio-temporal tokens extracted from the clip are forwarded to the model. This makes the transformer layer relate all pairs of interactions between tokens in space and time together, and therefore the long interactions between tokens throughout the video might require high computational complexity. For this reason, due to real-time computation concerns in visual odometry applications, we selected the encoder architecture with the “divided space-time” self-attention, which is more efficient in terms of processing complexity compared to the “joint space-time” self-attention. As the name suggests, it consists of applying attention along the time axis before the spatial one. Temporal attention uses tokens with the same spatial index, while spatial attention uses tokens from the

same frame.

The MLP head outputs the final estimated poses. Since two frames are required to estimate one pose, $N_f - 1$ poses are estimated from N_f frames. Therefore, the final MLP head has dimension $(N_f - 1) \times 6$, considering that we estimate the 6-DoF poses as being a 3D translation and 3D rotation with Euler angles, described in detail in Subsection 3.2. Note that our approach considers the information of all frames in the clip to infer a pose or multiple poses in the clip, depending on the number of frames.

As shown in Fig. 3, the encoder blocks comprise the layer normalization (LN), multi-head self-attention (MHSA), residual connections, fully connected layer (FC), and multilayer perceptron (MLP). Their simplified relation for the divided space-time architecture is given as follows:

$$\begin{aligned}
 \mathbf{a}_t^l &= \text{MHSA} \left(\text{LN} \left(\mathbf{z}_{(s,t)}^{l-1} \right) \right) + \mathbf{z}_{(s,t)}^{l-1}, \\
 \mathbf{a}_{t_{FC}}^l &= \text{FC} \left(\mathbf{a}_t^l \right), \\
 \mathbf{a}_s^l &= \text{MHSA} \left(\text{LN} \left(\mathbf{a}_{t_{FC}}^l \right) \right) + \mathbf{a}_{t_{FC}}^l, \\
 \mathbf{z}_{(s,t)}^l &= \text{MLP} \left(\text{LN} \left(\mathbf{a}_s^l \right) \right) + \mathbf{a}_s^l.
 \end{aligned} \tag{1}$$

The computation of the query (q), key (k), and value (v), input to the MSHA, is discussed in detail in [9, 14]. The multi-head self-attention has N_h attention heads computed in parallel, each one following Eq. (1).

We built the architectures based on the Data Efficient Image Transformer (DEIT) small [21], that is, with depth $L_x = 12$, MHSA component with $N_h = 6$ heads, and embedding dimension $E_d = 384$. The patch size was $P = 16$. The number of frames N_f in each clip impacts the number of parameters in the model since the output is a dense layer with $6(N_f - 1)$ neurons. The different models are defined in Table 1 according to their parameters.

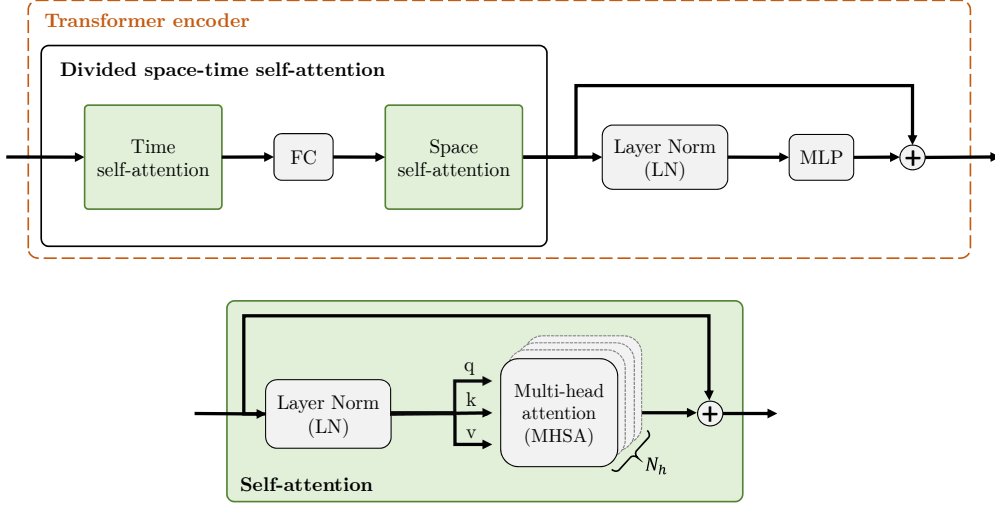


Figure 3: Transformer encoder with the divided space-time self-attention architecture.

3.2. Pre-processing

Pre-processing is an essential step when the data is labeled with global coordinates. In addition to the standard normalization using the training data statistics, i.e. subtracting the mean and dividing by the standard deviation, the pre-processing also comprises the conversion to relative coordinates and the correct angle notation.

3.2.1. Absolute to relative coordinates

In visual odometry, the motion $\mathbf{T}_k \in \mathbb{R}^{4 \times 4}$ is defined as

$$\mathbf{T}_k = \begin{bmatrix} \mathbf{R} & \mathbf{t} \\ \mathbf{0} & \mathbf{1} \end{bmatrix},$$

where k is the current time step, $\mathbf{R} \in SO(3)$ is the rotation matrix that describes the camera rotation, and $\mathbf{t} \in \mathbb{R}^{3 \times 1}$ is the translation vector. Both the rotation matrix and the translation vector depict the motion from time step $k-1$ to k .

The world absolute coordinates might not be useful for pose estimation, since we want to estimate the relative motion between consecutive frames. Let us assume we have the ground truth 3D local coordinates motion \mathbf{T}_{k-1} and \mathbf{T}_k . The pose of the camera at instant k relative to instant $k-1$, denoted as $\mathbf{T}_{k-1,k}$, is given by:

$$\mathbf{T}_{k-1,k} = \mathbf{T}_{k-1}^{-1} \mathbf{T}_k. \quad (2)$$

Table 1: TSformer-VO architectures.

Architecture	N_f	# Parameters
TSformer-VO-1	2	30,657,414
TSformer-VO-2	3	30,660,108
TSformer-VO-3	4	30,662,802

3.2.2. Rotation matrix to Euler angles

The rotations about the x , y , and z axes are referred to as roll, pitch, and yaw, respectively, and are denoted as ϕ , θ , and ψ , respectively. The rotation matrix \mathbf{R} can be expressed in terms of these rotations as follows:

$$\begin{aligned} \mathbf{R}(\phi, \theta, \psi) &= \begin{bmatrix} r_{11} & r_{12} & r_{13} \\ r_{21} & r_{22} & r_{23} \\ r_{31} & r_{32} & r_{33} \end{bmatrix} \\ &= \begin{bmatrix} c_\psi c_\theta & c_\psi s_\theta s_\phi - s_\psi c_\phi & s_\psi s_\theta s_\phi + c_\psi s_\theta c_\phi \\ s_\psi c_\theta & c_\psi c_\phi + s_\psi s_\theta s_\phi & s_\psi s_\theta c_\phi - c_\psi s_\phi \\ -s_\theta & c_\theta s_\phi & c_\theta c_\phi \end{bmatrix}, \end{aligned} \quad (3)$$

where $c_\alpha = \cos(\alpha)$ and $s_\alpha = \sin(\alpha)$, $\alpha \in \{\phi, \theta, \psi\}$. This representation follows the ZYX Euler parameterization, which yields the following Euler angles [22]:

$$\begin{aligned} \phi &= \text{atan2}(r_{21}, r_{11}), \\ \theta &= \text{atan2}\left(-r_{31}, \sqrt{r_{11}^2 + r_{21}^2}\right), \\ \psi &= \text{atan2}(r_{32}, r_{33}), \end{aligned} \quad (4)$$

where $\text{atan2}(y, x)$ is the two-argument arctan that returns the angle between the vector (x, y) and the x axis.

3.3. Post-processing

Post-processing involves recovering the global coordinates given the relative coordinates predicted by the model. For this purpose, the inverse operation of Eq. (2) can be applied, as well as transforming the Euler angles back to the rotation matrix. Moreover, the training

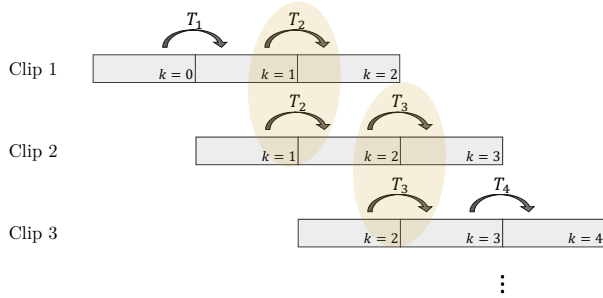


Figure 4: Visualization of the repeated motions, highlighted in yellow, for the particular case of $N_f = 3$ with 2 overlapped frames.

statistics used in normalizing the data should be reemployed to retrieve the denormalized estimated poses.

Furthermore, given the way we designed our problem, poses at the same time step can appear in different input clips. In our approach, we use input clips with N_f frames overlapped with $N_f - 1$ frames, as if a sliding window spans the video with stride 1. In other words, the clips act as a circular buffer of size N_f , and at each time step the oldest frame goes away and a new frame is appended to the clip. This overlap leads to the same pose being estimated with different input clips. Hence, we perform a minor adjustment by averaging all T_k motions over all clips where T_k appears given a time instant k . Fig. 4 helps with the visualization of the repeated motions in consecutive clips. Note that Fig. 4 shows a particular case for $N_f = 3$ with 2 overlapped frames. The repeated motions are highlighted in light yellow.

4. Experiments

4.1. Experimental setup

In the following, we detail the dataset with the evaluation metrics used to compare our approach with the state-of-the-art, the training hyperparameters, and the computation setup.

4.1.1. Dataset

We conduct our experiments with the KITTI odometry dataset [23], which is a benchmark for the development and evaluation of VO algorithms. The data is recorded at 10 frames per second by a stereo system mounted on a moving vehicle, capturing images while riding through streets and roads. Therefore, the scenes might contain pedestrians, parked and moving cars, bicycles, etc. In our case, since we deal with monocular VO, we only consider the images acquired by the left camera. The entire data has 22 sequences: 11 with

ground truth poses provided by a GPS for developing and evaluating the method, and 11 with no ground truth available. The length of the sequences is not equal, and the car speed varies from 0 to 90 km/h, making the VO challenging in high-speed and steep curve situations.

4.1.2. Evaluation metrics

We evaluate the methods using the KITTI odometry metrics defined below:

- t_{err} : average translational error, measured in percentage (%);
- r_{err} : average rotational error, measured in degrees per 100 meters ($^{\circ}/100$ m);
- ATE: absolute trajectory error, given in meters. It is the root mean squared error (RMSE) between the estimated camera pose and the ground truth;
- RPE: relative pose error for rotation and translation. It is measured frame-to-frame in degrees ($^{\circ}$) for the rotation, and in meters (m) for the translation.

The t_{err} and r_{err} are computed for all subsequences of length (100, 200, \dots , 800) meters, according to [23].

Monocular methods suffer from scale ambiguity while restoring the real-world scale. Prior works apply an optimization transformation to align the predicted poses to the ground truths. Therefore, we also applied a 7-DoF optimization in the validation step as it is typically done in the literature [24, 6]. The final metrics with the optimization were computed using the Python KITTI evaluation toolbox¹.

4.1.3. Loss function

The loss function used in this work is the mean squared error (MSE) between each predicted element and its ground truth target, defined as follows:

$$\mathcal{L}_{MSE} = \frac{1}{6B_s(N_f - 1)} \sum_{n=1}^{B_s} \sum_{i=1}^{6(N_f-1)} (\mathbf{y}_{i,n} - \hat{\mathbf{y}}_{i,n})^2, \quad (5)$$

where $\mathbf{y}_{i,n}$ is the 6-DoF relative poses ground truth of batch n , flattened into a column vector, and $\hat{\mathbf{y}}_{i,n}$ is its prediction by the model. For batch processing, the final loss is reduced by the mean over all B_s batch elements.

¹<https://github.com/Huangying-Zhan/kitti-odom-eval>

4.1.4. Training strategy

Out of the 11 KITTI sequences with ground truth, we used sequences 00, 02, 08, and 09 as training data, and 01, 03, 04, 05, 06, 07, and 10 as test data. We follow the choice made in [4] to conduct a fair comparison. Although only four sequences are used for training, they contain the largest recorded trajectories in the dataset. All the frames were resized to 192×640 to make the height and width dimensions multiples of the patch size ($P = 16$) while keeping the original aspect ratio of the dataset.

The input clips with N_f frames, $N_f \in \{2, 3, 4\}$, are sampled from the KITTI dataset. We sampled the clips using a sliding window of size N_f and stride 1. This means that consecutive clips have $N_f - 1$ overlapped frames. Next, we shuffle the sampled clips and organize them in batches of size 4. By doing this, we ensure that clips in the same batch are not sequential to each other. The batch size was picked according to our GPU memory capacity.

As validation data, we randomly select 10% of the training clips, so that the validation set has the same distribution as the training data. We compute the validation loss to do hyperparameter tuning and save the best model, i.e. the model with minimum validation loss during training.

The training procedure and the architectures were implemented with PyTorch 1.10. Computations were performed with a computer with a Intel i9-7900X CPU 3.3GHz CPU and a GeForce GTX 1080 Ti GPU with 11GB VRAM. We run experiments from scratch for 100 epochs with the Adam optimization to minimize the loss function. We set the learning rate to 1×10^{-5} and use the default values for the other parameters in the Adam algorithm. Fig. 5 shows the training and validation loss convergence curves obtained by training the architecture TSformer-VO-1.

4.2. Results

The qualitative and quantitative results of our TSformer-VO models are presented in the following. We also show the visualization of the learned spatio-temporal attention on the KITTI images, and the total computational time of our approach.

4.2.1. Comparison with the state-of-the-art

We conduct experiments to evaluate our approach by comparing it to other classical models in the literature. We evaluate the performance of our method by comparing it to ORB-SLAM2, which is a classical geometry-based method, and DeepVO, which is a famous deep learning-based method. We used the official

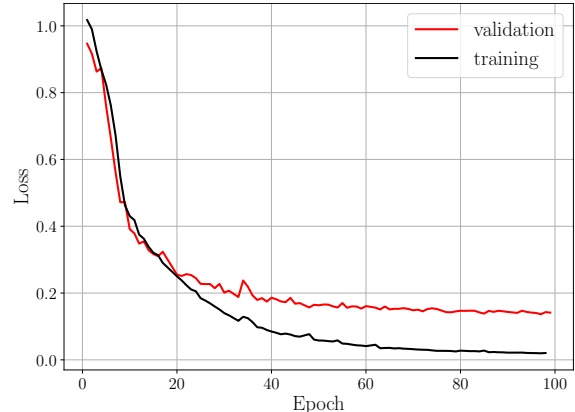


Figure 5: Training and validation loss curves of TSformer-VO-1 architecture.

C++ implementation of ORB-SLAM2² and the unofficial PyTorch implementation of DeepVO³. It is worth mentioning that the authors of DeepVO did not release the official code implementation. Therefore, we were very careful to choose the highest-rated unofficial PyTorch version available online on GitHub, also used in other related works [7, 25, 26, 27]. Furthermore, we do not apply loop closure on ORB-SLAM2 to keep a fair comparison between the algorithms, since DeepVO and TSformer-VO do not use loop detection to perform a pose-graph optimization.

The architectures defined in Table 1 were then trained and evaluated. The quantitative results are given in Table 2. The best values of each metric for each sequence are highlighted in bold, and the second best values are underlined.

To conduct a fair comparison among the methods, we must ignore the training sequences 00, 02, 08, and 09 as the learning nature of DeepVO and TSformer-VO is supervised, while ORB-SLAM2 is strictly geometric without a prior training step. That stated, we can see that the TSformer-VO model is competitive with the other state-of-the-art methods analyzed. ORB-SLAM2 is still superior with respect to metrics concerning rotations, such as r_{err} and RPE in ($^{\circ}$). However, TSformer-VO showed competitive results in translations, especially evident in sequences 01, 05, and 06 regarding the metrics t_{err} and RPE in meters.

Comparing algorithms of the same nature, i.e. based on deep learning, the three trained TSformer-VO architectures were clearly superior to the DeepVO method. This shows that transformer-based architectures can

²https://github.com/raulmur/ORB_SLAM2

³<https://github.com/ChiWeiHsiao/DeepVO-pytorch>

Table 2: Quantitative results of the selected models for the 11 KITTI sequences with ground truth.

Method	Sequence											
	00	01	02	03	04	05	06	07	08	09	10	
t_{err} (%)	ORB-SLAM2	9.938	107.565	12.396	1.554	1.554	9.671	18.899	10.195	11.456	10.031	3.638
	DeepVO	56.057	99.047	76.035	85.203	18.812	48.869	52.220	61.080	76.849	74.176	114.054
	TSformer-VO-1	4.392	37.322	5.587	14.731	8.242	9.623	25.053	17.013	5.078	3.512	15.459
	TSformer-VO-2	5.152	33.400	<u>4.870</u>	14.444	6.854	10.735	17.703	<u>23.205</u>	4.146	8.091	13.713
	TSformer-VO-3	4.649	<u>35.504</u>	4.737	<u>12.858</u>	<u>5.664</u>	12.588	28.973	22.959	4.238	<u>5.457</u>	<u>16.072</u>
r_{err} (°/100m)	ORB-SLAM2	0.583	0.888	0.278	0.182	0.267	0.243	0.234	0.327	0.283	0.287	0.322
	DeepVO	34.118	12.930	31.252	24.602	7.176	35.305	33.569	59.860	33.435	32.005	26.632
	TSformer-VO-1	1.811	5.321	<u>1.269</u>	6.988	4.849	<u>3.629</u>	8.443	<u>6.361</u>	1.969	<u>1.133</u>	4.670
	TSformer-VO-2	2.169	6.251	1.415	6.129	3.556	4.002	5.622	9.992	1.624	1.973	5.111
	TSformer-VO-3	1.898	<u>5.192</u>	1.567	<u>5.756</u>	<u>3.492</u>	5.133	8.838	11.544	1.671	2.088	5.161
ATE (m)	ORB-SLAM2	42.055	502.201	57.382	1.752	1.296	33.196	55.025	<u>16.557</u>	43.088	41.746	7.735
	DeepVO	95.919	68.258	150.559	21.021	5.648	54.860	88.468	7.961	68.191	30.700	22.755
	TSformer-VO-1	51.083	<u>126.225</u>	42.122	16.623	4.750	46.890	78.820	32.883	<u>41.859</u>	18.815	22.975
	TSformer-VO-2	50.066	209.038	62.188	14.737	4.244	54.688	50.519	36.059	28.534	41.126	21.131
	TSformer-VO-3	<u>46.521</u>	160.546	<u>55.242</u>	<u>14.152</u>	<u>3.057</u>	61.387	88.314	31.490	26.466	23.683	<u>22.696</u>
RPE (m)	ORB-SLAM2	0.142	2.970	0.199	0.033	0.078	0.147	0.300	0.112	0.192	0.145	0.055
	DeepVO	0.610	2.277	1.155	0.666	0.337	0.605	0.838	0.524	0.811	0.831	1.002
	TSformer-VO-1	0.026	1.007	0.073	0.134	0.086	0.142	0.326	0.136	0.025	0.032	0.148
	TSformer-VO-2	<u>0.028</u>	0.751	<u>0.053</u>	<u>0.128</u>	<u>0.083</u>	0.144	0.209	0.143	0.032	0.092	0.145
	TSformer-VO-3	0.032	<u>0.953</u>	0.038	0.134	0.112	0.139	0.404	0.162	<u>0.030</u>	<u>0.044</u>	0.154
RPE (°)	ORB-SLAM2	0.078	0.098	<u>0.072</u>	0.053	0.079	0.057	0.057	0.049	0.061	0.063	0.067
	DeepVO	1.039	0.624	0.922	0.567	0.171	0.716	0.610	0.940	0.872	0.969	0.746
	TSformer-VO-1	0.230	0.284	0.195	0.230	0.155	0.213	0.208	0.230	0.185	0.160	0.285
	TSformer-VO-2	<u>0.364</u>	<u>0.751</u>	0.053	0.128	<u>0.083</u>	0.144	<u>0.209</u>	0.143	0.032	<u>0.092</u>	<u>0.145</u>
	TSformer-VO-3	0.368	0.294	0.288	0.292	0.173	0.279	0.264	0.322	0.283	0.236	0.333

also provide high performance in visual odometry tasks. As an example, the DeepVO only shows scores higher than TSformer-VO-2 for the ATE of sequences 01, 07, and 09, and RPE (°) for sequence 01. For all the remaining metrics and sequences, the TSformer-VO-2 outperforms the DeepVO.

A qualitative analysis is shown in Fig. 6. The predicted trajectories are displayed on top of each other together with the expected ground truth. In Fig. 6, it can be seen that there is a scale drift problem, which is expected in monocular odometry systems. It is worth noting that ORB-SLAM2 had the worst performance in sequence 01 mainly due to the high-speed scenario in this sequence, hindering the tracking of features along the frames with classical matching and tracking algorithms. This issue is not found in DeepVO and TSformer-VO, revealing an advantage of deep learning-based methods over geometry-based ones in high-speed scenarios.

Furthermore, we observed in our experiments that the DeepVO and TSformer-VO methods are able to estimate better poses in terms of translation without the 7-DoF alignment required by the ORB-SLAM2, as shown in Figure 7. This result is favorable for the choice of deep learning-based methods over geometry-based methods, as deep learning indirectly captures the scale in the data during training.

4.2.2. Visualization of the learned space-time attention

Understanding what the network is learning might be valuable information to further improve the method. The learned space-time attention can be visualized with the Attention Rollout introduced in [28]. This method shows which part of the input is considered important to the network after training. The idea is to propagate the attention weights through the layers quantifying the flow of information. Fig. 8 shows the visualization of the space-time attention for examples of the KITTI dataset.

Fig. 8 illustrates an example where the learned attention focus on the static scene, ignoring moving objects such as the cars. The learned attention disregards both cars moving in the same direction as the camera and those moving in the opposite direction. This behavior was frequently observed in the KITTI sequences, indicating the network’s ability to ignore moving objects and extract relevant features from static scenarios. In addition, differently from classical approaches based on keypoint detectors, the learned space-time attention has blob shapes, giving preference to regions instead of corners. This can be advantageous as it is easier to track larger objects rather than single keypoints given the number of pixels available in the objects.

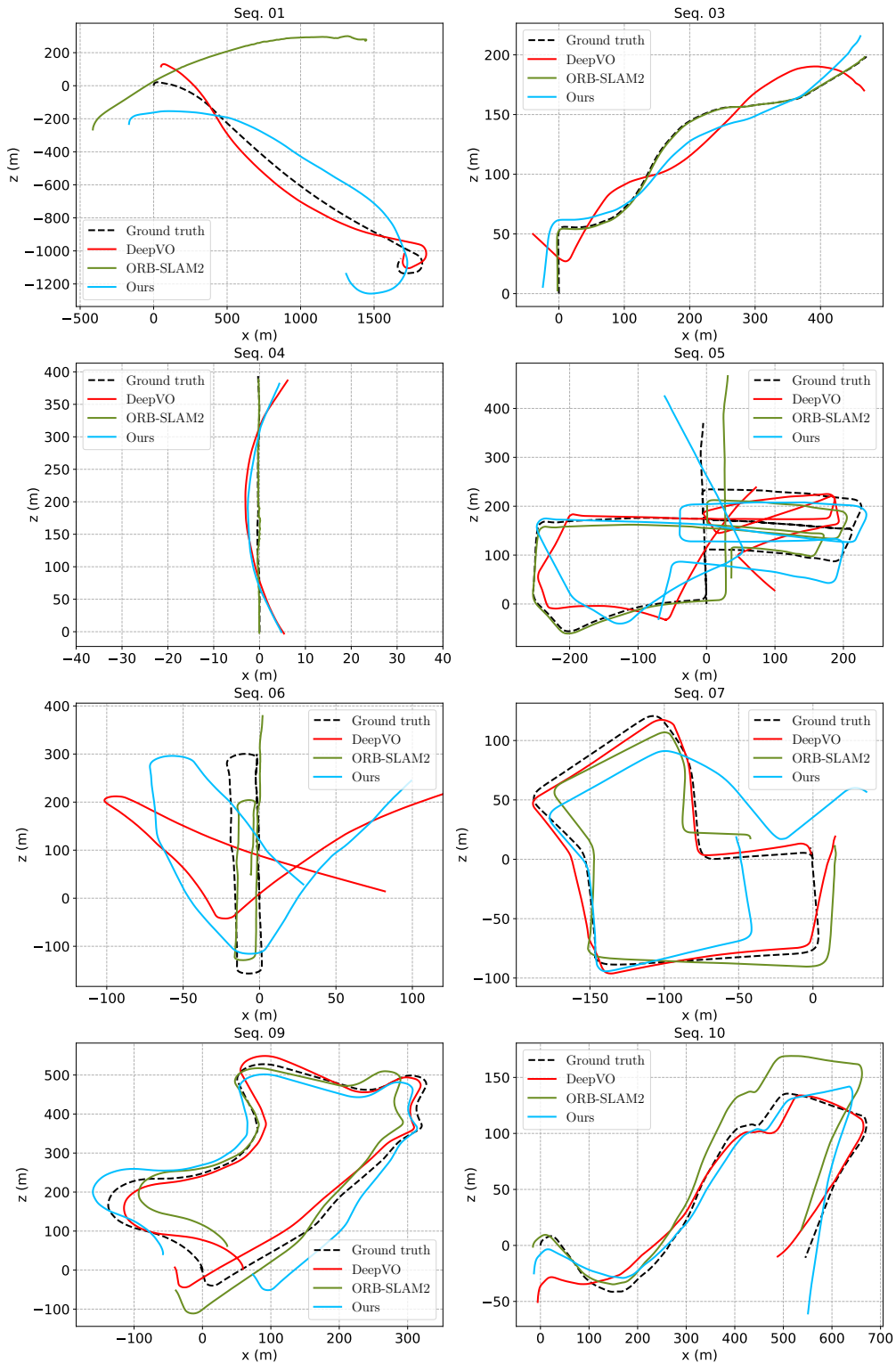


Figure 6: Trajectories obtained by the ORB-SLAM2(■), DeepVO (■), and TSformer-VO-2 (■), compared with the ground truth (■) in sequences 01, 03, 04, 05, 06, 07, 09, and 10 of the KITTI odometry dataset. The depicted sequences belong to the test set, except sequence 09, and the trajectories are obtained under the 7-DoF alignment.

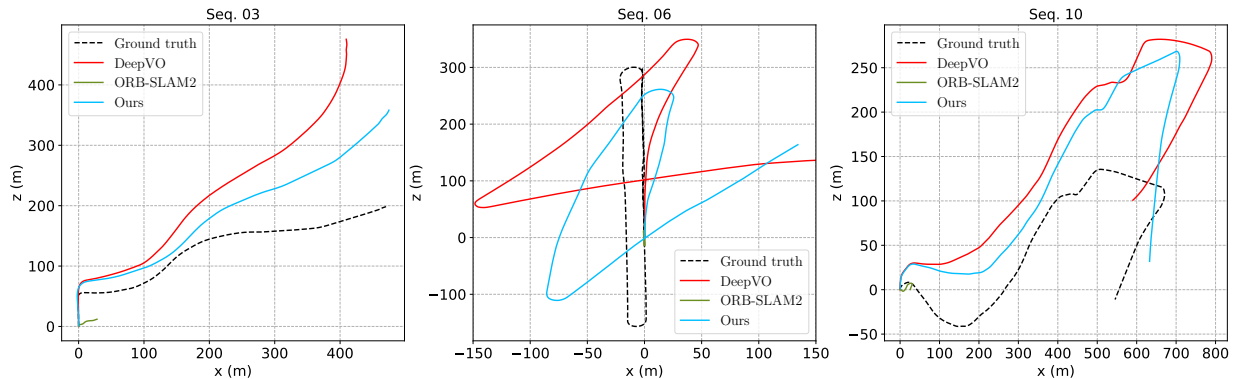


Figure 7: Trajectories without the 7-DoF alignment obtained by the ORB-SLAM2 (■), DeepVO (■), and TSformer-VO-2 (■), compared with the ground truth (■) in sequences 03, 06, and 10 of the KITTI odometry dataset.

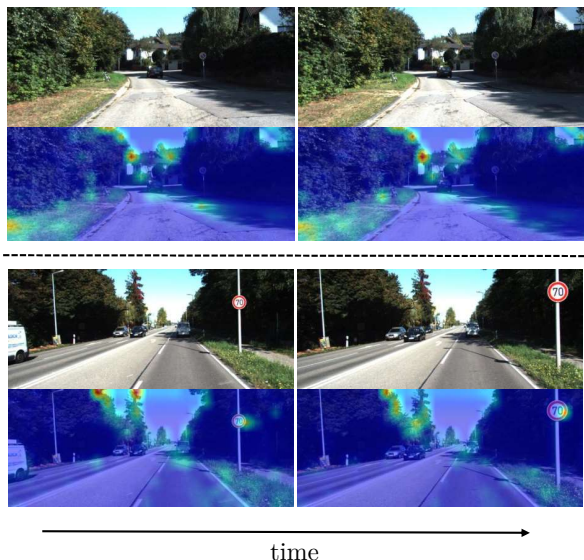


Figure 8: Visualization of the learned space-time attention in the context of visual odometry using the KITTI dataset.

4.2.3. Computational time for TSformer-VO

Considering the importance of real-time processing for visual odometry, we measured the inference time of our proposed models. We computed the mean computational time and its standard deviation required for our models to estimate the poses in 1100 clips. Table 3 shows the average inference time for each model, using the computer described in Subsection 4.1.4.

The pre- and post-processing require on average 3.369 ms, and 0.031 ms, respectively, to process a pair of frames. Note that for the test case, the pre-processing step consists only of data normalization and resizing. For a system operating at 10 frames per second, as in the

Table 3: Comparison of inference times for TSformer-VO models per clip.

Model	mean (ms)	std. dev. (ms)
TSformer-VO-1	20.346	0.032
TSformer-VO-2	28.840	0.505
TSformer-VO-3	37.877	0.822

KITTI benchmark, the sample time to capture one frame is 100 ms. Table 3 gives that our approach requires an inference time between 20 ms and 40 ms on average with our computational setup. Therefore, regarding processing time, even our largest model (TSformer-VO-3) is capable of real-time application once the total processing time is lower than the sample time.

Notice that despite our method requiring N_f frames, we do not need to wait for N_f frames to be captured before an inference, since we can keep a buffer with the last $N_f - 1$ frames and complete it with the current frame. Then, as a new frame arrives, the oldest one is dropped from this buffer while the new frame is added. The average motion computed between relative pose estimates suggested in Subsection 3.3 as a post-processing step is advised for high-accuracy applications. However, for low latency applications, such as control systems, this average process may be skipped to avoid introducing delay.

5. Conclusion

Finally, our experiments have shown that a Transformer-based model originally created for video understanding problems can predict the 6-DoF camera’s pose given sequential images as input. We trained and evaluated different architectures varying the

last dense layer and the number of frames of the input clips. Our results showed that the trained TSformer-VO models achieved competitive results in the KITTI dataset when compared to state-of-the-art methods based on deep learning and geometry, respectively DeepVO and ORB-SLAM2. Considering only the deep learning-based method, the rotation and translation metrics support that our approach was superior to the DeepVO implementation widely accepted in the community. Furthermore, we observed that the learned spatio-temporal attention is mostly drawn to the static scene, which is desirable in visual odometry tasks. We also show that our approach enables real-time processing even for our largest model.

In addition, even with a relatively small dataset such as the KITTI, the model managed to estimate the camera’s poses achieving results on par with the state-of-the-art. Due to its deep learning nature, the larger the amount of data the better the learning during training. Therefore, we expect to increase the model’s performance by using larger datasets and transfer learning techniques. Furthermore, one can explore our approach based on unsupervised learning in a similar manner as done in [5], as well as experiment novel cost functions that leverage the consistency among repeated motions in consecutive overlapped clips.

CRediT authorship contribution statement

André Françani: Conceptualization, Methodology, Software, Validation, Investigation, Writing-original-draft. **Marcos Maximo:** Conceptualization, Writing-review-editing, Supervision.

Data availability

The KITTI odometry dataset used as the benchmark is available online. Code is available online at <https://github.com/aofrancani/TSformer-VO>.

Declaration of competing interest

The authors declare that they have no known competing financial interests or personal relationships that could have appeared to influence the work reported in this paper.

Acknowledgments

André Françani was supported by CAPES – Coordination of Improvement of Higher Education Personnel

under grant 88887.687888/2022-00. Marcos Maximo is partially funded by CNPq — National Research Council of Brazil through grant 307525/2022-8.

References

- [1] D. Scaramuzza, F. Fraundorfer, Visual odometry [tutorial], *IEEE Robotics & Automation Magazine* 18 (4) (2011) 80–92.
- [2] A. Geiger, J. Ziegler, C. Stiller, StereoScan: Dense 3D reconstruction in real-time, in: *Intelligent Vehicles Symposium (IV)*, 2011.
- [3] C. Campos, R. Elvira, J. J. G. Rodríguez, J. M. M. Montiel, J. D. Tardós, ORB-SLAM3: An accurate open-source library for visual, visual-inertial and multi-map SLAM, *IEEE Transactions on Robotics* 37 (6) (2021) 1874–1890.
- [4] S. Wang, R. Clark, H. Wen, N. Trigoni, DeepVO: Towards end-to-end visual odometry with deep recurrent convolutional neural networks, in: *2017 IEEE international conference on robotics and automation (ICRA)*, IEEE, 2017, pp. 2043–2050.
- [5] R. Li, S. Wang, Z. Long, D. Gu, UnDeepVO: Monocular visual odometry through unsupervised deep learning, in: *2018 IEEE international conference on robotics and automation (ICRA)*, IEEE, 2018, pp. 7286–7291.
- [6] H. Zhan, C. S. Weerasekera, J.-W. Bian, I. Reid, Visual odometry revisited: What should be learnt?, in: *2020 IEEE International Conference on Robotics and Automation (ICRA)*, IEEE, 2020, pp. 4203–4210.
- [7] H. M. S. Bruno, E. L. Colombini, LIFT-SLAM: A deep-learning feature-based monocular visual SLAM method, *Neurocomputing* 455 (2021) 97–110.
- [8] A. O. Françani, M. R. Maximo, Dense prediction transformer for scale estimation in monocular visual odometry, *arXiv preprint: 2210.01723* (2022).
- [9] A. Vaswani, N. Shazeer, N. Parmar, J. Uszkoreit, L. Jones, A. N. Gomez, Ł. Kaiser, I. Polosukhin, Attention is all you need, *Advances in Neural Information Processing Systems* 30 (2017).
- [10] J. Devlin, M.-W. Chang, K. Lee, K. Toutanova, BERT: Pre-training of deep bidirectional transformers for language understanding, *arXiv preprint: 1810.04805* (2018).
- [11] A. Radford, K. Narasimhan, T. Salimans, I. Sutskever, et al., Improving language understanding by generative pre-training (2018).
- [12] A. Dosovitskiy, L. Beyer, A. Kolesnikov, D. Weissenborn, X. Zhai, T. Unterthiner, M. Dehghani, M. Minderer, G. Heigold, S. Gelly, et al., An image is worth 16x16 words: Transformers for image recognition at scale, *arXiv preprint: 2010.11929* (2020).
- [13] A. Arnab, M. Dehghani, G. Heigold, C. Sun, M. Lučić, C. Schmid, ViViT: A video vision transformer, in: *Proceedings of the IEEE/CVF International Conference on Computer Vision (ICCV)*, 2021, pp. 6836–6846.
- [14] G. Bertasius, H. Wang, L. Torresani, Is space-time attention all you need for video understanding?, in: *Proceedings of the International Conference on Machine Learning (ICML)*, 2021.
- [15] A. Geiger, J. Ziegler, C. Stiller, StereoScan: Dense 3D reconstruction in real-time, in: *Intelligent Vehicles Symposium (IV)*, 2011.
- [16] R. Mur-Artal, J. M. M. Montiel, J. D. Tardós, ORB-SLAM: A versatile and accurate monocular SLAM system, *IEEE Transactions on Robotics* 31 (5) (2015) 1147–1163. doi:10.1109/TR0.2015.2463671.
- [17] A. Dosovitskiy, P. Fischer, E. Ilg, P. Hausser, C. Hazirbas, V. Golkov, P. Van Der Smagt, D. Cremers, T. Brox, FlowNet:

- Learning optical flow with convolutional networks, in: Proceedings of the IEEE international conference on computer vision, 2015, pp. 2758–2766.
- [18] C. Feichtenhofer, H. Fan, J. Malik, K. He, SlowFast networks for video recognition, in: Proceedings of the IEEE/CVF International Conference on Computer Vision, 2019, pp. 6202–6211.
- [19] C. Feichtenhofer, X3D: Expanding architectures for efficient video recognition, in: Proceedings of the IEEE/CVF Conference on Computer Vision and Pattern Recognition, 2020, pp. 203–213.
- [20] A. Arnab, M. Dehghani, G. Heigold, C. Sun, M. Lučić, C. Schmid, ViViT: A video vision transformer, in: Proceedings of the IEEE/CVF International Conference on Computer Vision, 2021, pp. 6836–6846.
- [21] H. Touvron, M. Cord, M. Douze, F. Massa, A. Sablayrolles, H. Jegou, Training data-efficient image transformers & distillation through attention, in: International Conference on Machine Learning, Vol. 139, 2021, pp. 10347–10357.
- [22] K. M. Lynch, F. C. Park, Modern robotics, Cambridge University Press, 2017.
- [23] A. Geiger, P. Lenz, R. Urtasun, Are we ready for autonomous driving? the KITTI vision benchmark suite, in: Conference on Computer Vision and Pattern Recognition (CVPR), 2012.
- [24] R. Mur-Artal, J. D. Tardós, ORB-SLAM2: An open-source SLAM system for monocular, stereo, and RGB-D cameras, IEEE Transactions on Robotics 33 (5) (2017) 1255–1262. doi: 10.1109/TR0.2017.2705103.
- [25] S. Chen, K. Mai, Towards specialized hardware for learning-based visual odometry on the edge, in: 2022 IEEE/RSJ International Conference on Intelligent Robots and Systems (IROS), 2022, pp. 10603–10610. doi:10.1109/IROS47612.2022.9982046.
- [26] N. Kaygusuz, O. Mendez, R. Bowden, MDN-VO: Estimating visual odometry with confidence, in: 2021 IEEE/RSJ International Conference on Intelligent Robots and Systems (IROS), IEEE, 2021, pp. 3528–3533.
- [27] N. Kaygusuz, O. Mendez, R. Bowden, AFT-VO: Asynchronous fusion transformers for multi-view visual odometry estimation, in: 2022 IEEE/RSJ International Conference on Intelligent Robots and Systems (IROS), IEEE, 2022, pp. 2402–2408.
- [28] S. Abnar, W. Zuidema, Quantifying attention flow in transformers, arXiv preprint arXiv:2005.00928 (2020).